OPEN

Oncogene (2017) **36,** 6049–6058

www.nature.com/onc

ORIGINAL ARTICLE

Inhibition of colony stimulating factor-1 receptor abrogates microenvironment-mediated therapeutic resistance in gliomas

D Yan[1], J Kowal[2,3], L Akkari[1,2,3], AJ Schuhmacher[1], JT Huse[4], BL West[5] and JA Joyce[1,2,3]

Glioblastomas represent the most aggressive glioma grade and are associated with a poor patient prognosis. The current standard of care, consisting of surgery, radiation and chemotherapy, only results in a median survival of 14 months, underscoring the importance of developing effective new therapeutic strategies. Among the challenges in treating glioblastomas are primary resistance and the rapid emergence of recurrent disease, which can result from tumor cell-intrinsic mechanisms in addition to tumor microenvironment (TME)-mediated extrinsic resistance. Using a PDGF-B-driven proneural glioma mouse model, we assessed a panel of tyrosine kinase inhibitors with different selectivity profiles. We found that PLX3397, an inhibitor of colony stimulating factor-1 receptor (CSF-1R), blocks glioma progression, markedly suppresses tumor cell proliferation and reduces tumor grade. By contrast, the multi-targeted tyrosine kinase inhibitors dovitinib and vatalanib, which directly target tumor cells, exert minimal anti-tumoral effects *in vivo*, despite killing glioma cells *in vitro*, suggesting a TME-mediated resistance mechanism may be involved. Interestingly, PLX3397 interferes with tumor-mediated education of macrophages and consequently restores the sensitivity of glioma cells to tyrosine kinase inhibitors *in vivo* in preclinical combination trials. Our findings thus demonstrate that microenvironmental alteration by CSF-1R blockade renders tumor cells more susceptible to receptor tyrosine kinase inhibition in a preclinical glioblastoma model, which may have important translational relevance.

Oncogene (2017) **36,** 6049–6058; doi:10.1038/onc.2017.261; published online 31 July 2017

INTRODUCTION

Glioblastomas are the most aggressive type of glioma and are associated with a poor patient prognosis across all molecular subtypes.[1,2] Despite some progress in neurosurgery, radiotherapy and chemotherapy treatment options, patient survival has improved only marginally during the past three decades. Under the current standard of care regimen, which consists of surgery, radiation and chemotherapy with the alkylating agent temozolomide, the median survival for patients diagnosed with glioblastoma is just 14.6 months.[1] Therefore, this disease poses a significant challenge for contemporary healthcare, and novel therapeutics are urgently required to address the unmet medical needs.

The aggressiveness of glioblastoma is driven both by genetic aberrations in glioma cells and alterations to the tumor microenvironment (TME).[3,4] Genetic changes such as *PDGFRA* amplification, *TP53* loss, *NF1* loss and *EGFR* mutation activate mitogenic pathways, causing tumor cells to rapidly proliferate.[5] Although considerable effort has been directed towards inhibiting aberrantly activated signaling pathways in glioma cells,[6] success remains limited. A wide range of receptor tyrosine kinase (RTK) inhibitors, predominantly targeting PDGFR and EGFR, has been used to interfere with pro-proliferative and pro-invasive pathways in gliomas. These inhibitors show variable preclinical efficacy but universally suffer from insufficient clinical activity. For example, the PDGFR inhibitor imatinib showed promising anti-tumor activities in preclinical studies but failed to deliver significant survival improvement in patients with recurrent glioblastoma.[7,8] The failure of these trials can likely be attributed to the fact that multiple mechanisms are employed in glioblastoma to achieve primary and acquired drug resistance. Several tumor cell-intrinsic processes that mediate unresponsiveness to different treatments have been identified to date, including activation of anti-apoptosis pathways,[9] bypass signaling,[10] enrichment of glioma-initiating cells[11,12] and drug efflux machinery,[13] among others. A glioma cell-centric therapy thus needs to evade or overcome numerous such processes in order to achieve a durable response, which is challenging from a drug development perspective.

Therapeutic targeting of the glioma microenvironment, by contrast, could be expected to represent a more tractable strategy. Compared with tumor cells, non-neoplastic stromal and immune cells are genomically stable, and are thus less prone to the development of resistance and subsequent rapid clonal evolution, a phenomenon linked to therapeutic failure.[14] The glioblastoma TME contains diverse populations of non-cancerous cells, including resident microglia, recruited macrophages, immature myeloid cells, astrocytes, T cells, and endothelial cells, among others.[4,15,16] These cells are either inhibited in the immunosuppressive TME or actively engage in pro-tumorigenic activities.[17] Notably, increasing evidence has demonstrated that tumor-associated microglia and macrophages (TAMs) contribute to glioma progression by enforcing immunosuppression and enhancing proliferation, invasion and angiogenesis.[4,18] Moreover, TAMs can represent up to 30% of the glioblastoma mass,[19,20] and TAM-associated gene expression is significantly associated with reduced patient survival.[21] These findings underscore the

[1]Cancer Biology and Genetics Program, Memorial Sloan Kettering Cancer Center, New York, NY, USA; [2]Ludwig Institute for Cancer Research, University of Lausanne, Lausanne, Switzerland; [3]Department of Oncology, University of Lausanne, Lausanne, Switzerland; [4]Departments of Pathology and Translational Molecular Pathology, University of Texas MD Anderson Cancer Center, Houston, TX, USA and [5]Plexxikon Inc., Berkeley, CA, USA. Correspondence: Professor JA Joyce, Department of Oncology, University of Lausanne, Vaud, Lausanne 1066, Switzerland.
E-mail: johanna@joycelab.org
Received 29 January 2017; revised 31 May 2017; accepted 23 June 2017; published online 31 July 2017

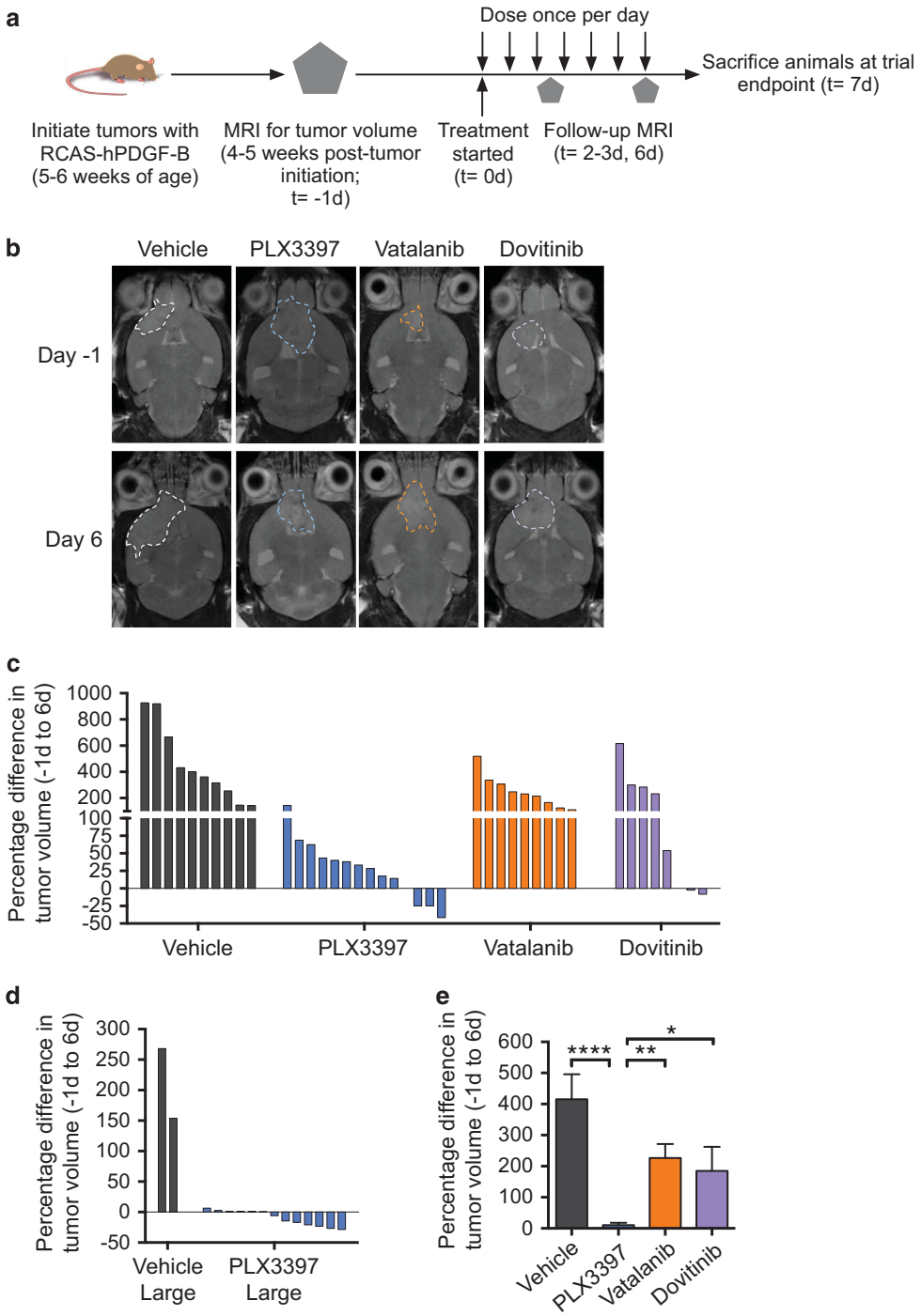

Figure 1. Preclinical tyrosine kinase inhibitor trials in the PDG model. (**a**) Tumor growth was monitored by schematic representation of trial design. (**b**) Representative magnetic resonance images of treated gliomas on day − 1 and day 6, indicated by dashed lines. (**c**) Waterfall plot showing a summary of tumor volume changes in all treatment arms: vehicle ($n = 10$), PLX3397 ($n = 14$), dovitinib ($n = 8$), vatalanib ($n = 10$), with an initial tumor volume of < 40 mm^3 at the beginning of the trial. (**d**) Waterfall plot showing a summary of tumor volume changes in vehicle ($n = 2$) and PLX3397 ($n = 13$) arms, with an initial tumor volume > 40 mm^3. Vehicle large: gliomas with > 40 mm^3 starting volume treated with vehicle; PLX3397 Large: gliomas with > 40 mm^3 starting volume treated with PLX3397. (**e**) Percentage differences in tumor volume in all treatment arms shown in Figures 1c and d. One-way analysis of variance with Sidak's multiple comparisons test was used to calculate statistical significance. $^*P < 0.05$; $^{**}P < 0.01$; $^{****}P < 0.0001$.

importance of TAM functions in glioblastoma, and provide a strong rationale for therapeutically targeting this cell population.

Previously, we reported that inhibition of colony stimulating factor-1 receptor (CSF-1R), using the small molecule BLZ945, alters the functions of TAMs and thus blocks proneural glioblastoma progression.[22] These data indicate that re-education of TAMs is a potent therapeutic strategy against glioblastoma and should be further assessed in single-agent or adjuvant/ neoadjuvant settings. However, questions remain as to the relative benefits of such a TME-targeting strategy versus traditional tumor cell-targeted therapies. Therefore, in the current study we directly compared these therapeutic options

as single agents and in combination to target both the tumor and its supportive microenvironment.

RESULTS

CSF-1R inhibition blocks the progression of established proneural gliomas

To directly compare the therapeutic efficacy of CSF-1R inhibitors with multi-targeted tyrosine kinase inhibitors, we selected PLX3397, a potent CSF-1R and c-Kit inhibitor[23] with demonstrated clinical benefit in synovial diffuse-type giant cell tumors,[24] as well as vatalanib and dovitinib, two inhibitors targeting multiple RTKs. Vatalanib inhibits PDGFR-β, VEGFR1/2/3, c-Kit and CSF-1R to varying degrees of efficacy,[25] and dovitinib inhibits Flt3, c-Kit, FGFR1/3, VEGFR1/2/3, PDGFR-β and CSF-1R to different extents.[26] For both drugs, substantially higher effective concentrations are required for effective CSF-1R inhibition compared with their other RTK targets. To conduct preclinical trials, we chose the immunocompetent PDGF-B-driven glioma (PDG) genetically engineered mouse model. In these mice, Nestin$^+$ glioma-initiating cells express the receptor for the replication-competent avian retrovirus, thus allowing cell type-specific delivery of the oncogene *PDGF-B*[27] in an *Ink4a/Arf*-deficient background. We previously showed that CSF-1R expression is restricted to TAMs, and PDGFR-α expression is glioma cell-specific.[22] Further analysis of the TME by immunostaining of PDG tumors herein revealed that a small proportion of CD31$^+$ endothelial cells express VEGFR2 (Supplementary Figure S1A) and low levels of c-Kit (Supplementary Figure S1B). In addition, a very small percentage of glioma cells express low levels of c-Kit (Supplementary Figure S1B). Consistent with the scarcity of evident c-Kit expression in glioma cells *in vivo*, we did not detect *Kit* expression in PDGC23, a representative glioma cell line derived from the PDG model[22] nor the human glioma cell line U-87MG (data not shown). There was also no evident expression of c-Kit or VEGFR2 in CD68$^+$ TAMs by immunostaining (Supplementary Figures S1A and B).

To determine the effect of the RTK inhibitors on established high-grade gliomas, mice with an initial tumor volume of $\leqslant 40\,mm^3$ were randomized into the vehicle arm or individual inhibitor arms, such that animals with equivalent tumor volumes were distributed comparably between the groups, and orally dosed daily for 7 consecutive days. Tumor volume was monitored by magnetic resonance imaging scans on day −1 and day 6 (Figure 1a). On the basis of published studies, we selected the dosages of inhibitors to satisfy three criteria: (i) equivalent molar quantities of drugs should be administered to allow for fair comparison of their efficacy; (ii) therapeutic responses had been documented in preclinical models of other tumor types using similar dosages; and (iii) toxicity must be minimal.[28–30] Pharmacokinetic analyses showed that all three compounds readily entered the systemic circulation and were detectable in the brain parenchyma 2 h following oral administration (Supplementary Figure S1C). In the vehicle arm, all gliomas progressed, ranging from 150 to 930% increase in tumor burden during the 7-day trial (Figures 1b and c). Vatalanib or dovitinib treatment resulted in only modest growth inhibition, with at least 50% of animals showing a similar growth rate to vehicle-treated tumors (Figures 1b and c). By contrast, PLX3397-treated gliomas showed either tumor regression or considerably slower growth, ranging from −40 to +140% respectively (Figures 1b and c).

Given the relative efficacy of PLX3397, we treated an additional cohort of mice harboring an initial tumor volume of $>40\,mm^3$ (denoted as 'PLX3397 Large') with PLX3397. Tumor volume-matching with a vehicle cohort of an equal size was not feasible, because most vehicle-treated mice would not survive the 7-day trial period due to the greater starting tumor burden, compared to the trial described above. The vehicle-treated mice ($>40\,mm^3$ initial tumor volume) that did survive had appreciable tumor growth, ranging from 150 to 270%, whereas PLX3397-treated mice showed either evident tumor regression or halted tumor growth, ranging from −30 to +6% (Figure 1d). Statistical analysis of all groups (from Figure 1c) revealed that PLX3397 decreased glioma growth by 97.5% compared to the vehicle group (Figure 1e; $P < 0.0001$). By comparison, vatalanib and dovitinib reduced growth by 45.6 and 55.6%, respectively (Figure 1e), highlighting the superior preclinical efficacy of PLX3397 in proneural gliomas.

The minimal efficacy of vatalanib and dovitinib raised the question as to whether these drugs indeed inhibited the intended molecular targets. Therefore, we analyzed protein fractions from treated whole tumors by immunoblotting for phosphorylated (p) CSF-1R and PDGFR-α. When adjusted to total receptor levels, PLX3397 potently inhibited CSF-1R phosphorylation, whereas vatalanib and dovitinib exerted modest effects (Supplementary Figure S1D). PDGFR-α phosphorylation was effectively inhibited by both vatalanib and dovitinib (Supplementary Figure S1D), while the effect of PLX3397 on PDGFR-α phosphorylation could not be assessed due to very low numbers of PDGFR-α-positive tumor cells in the efficiently debulked gliomas (Supplementary Figure S1D, lower panels). These data demonstrate that all three inhibitors efficiently act on their molecular targets *in vivo*. Of note, while PLX3397 has reported affinity to c-Kit, given that c-Kit expression was observed in only some endothelial cells, a very small number of glioma cells, and undetectable on TAMs (Supplementary Figure S1B, and data not shown), we consider it unlikely that c-Kit inhibition accounts for the robust anti-glioma activity of PLX3397 *in vivo* in the animal model used here.

To examine the effect of the inhibitors directly on target cells, we explored the dose–response relationship of individual inhibitors using the murine PDGC23 glioma cell line, the human U-87MG glioma cell line, mouse primary bone marrow-derived macrophages (BMDMs) and human monocyte-derived macrophages (MDMs). PLX3397 had no effect on the survival of murine glioma cells, whereas vatalanib and dovitinib reduced cell viability at micromolar concentrations (Supplementary Figure S2A). On the other hand, human U87 cells were killed by dovitinib, were relatively insensitive to vatalanib, and not significantly affected by PLX3397 (Supplementary Figure S2A). In murine glioma cells, this inhibitory effect appears to depend on PDGFR signaling, as addition of PDGF-BB markedly increased the cellular IC_{50} in PDGC23 cells (Supplementary Figure S2B). In murine BMDMs and human MDMs, PLX3397 efficiently decreased cell viability, while approximately 10-fold higher concentrations were required for vatalanib and dovitinib to achieve similar effects (Supplementary Figure S2C). This difference is also evident by immunoblotting analysis where PLX3397, but neither vatalanib nor dovitinib, successfully abolished CSF-1R phosphorylation at nanomolar concentrations (Supplementary Figures S3A and B).

Changes in glioma cell viability can be caused by altered cell cycle status, cell death or a combination of both. Cell cycle analysis of dovitinib-treated PDGC23 glioma cells in culture revealed a prominent G2-arrested subpopulation that was rapidly induced by the inhibitor and persisted throughout the experimental time course (Supplementary Figures S4A and E). Dovitinib progressively elevated cell death, killing up to 55% of cells at the assay end point (Supplementary Figure S4B; $P < 0.0001$). Vatalanib diminished the S-phase subpopulation without inducing G2 arrest (Supplementary Figures S4C and F), and killed ~35% of cells at the cellular IC_{50} (Supplementary Figure S4D; $P < 0.0001$). These data suggest that both vatalanib and dovitinib regulate glioma cell cycle and cell death, and dovitinib is a more potent anti-proliferation agent *in vitro*.

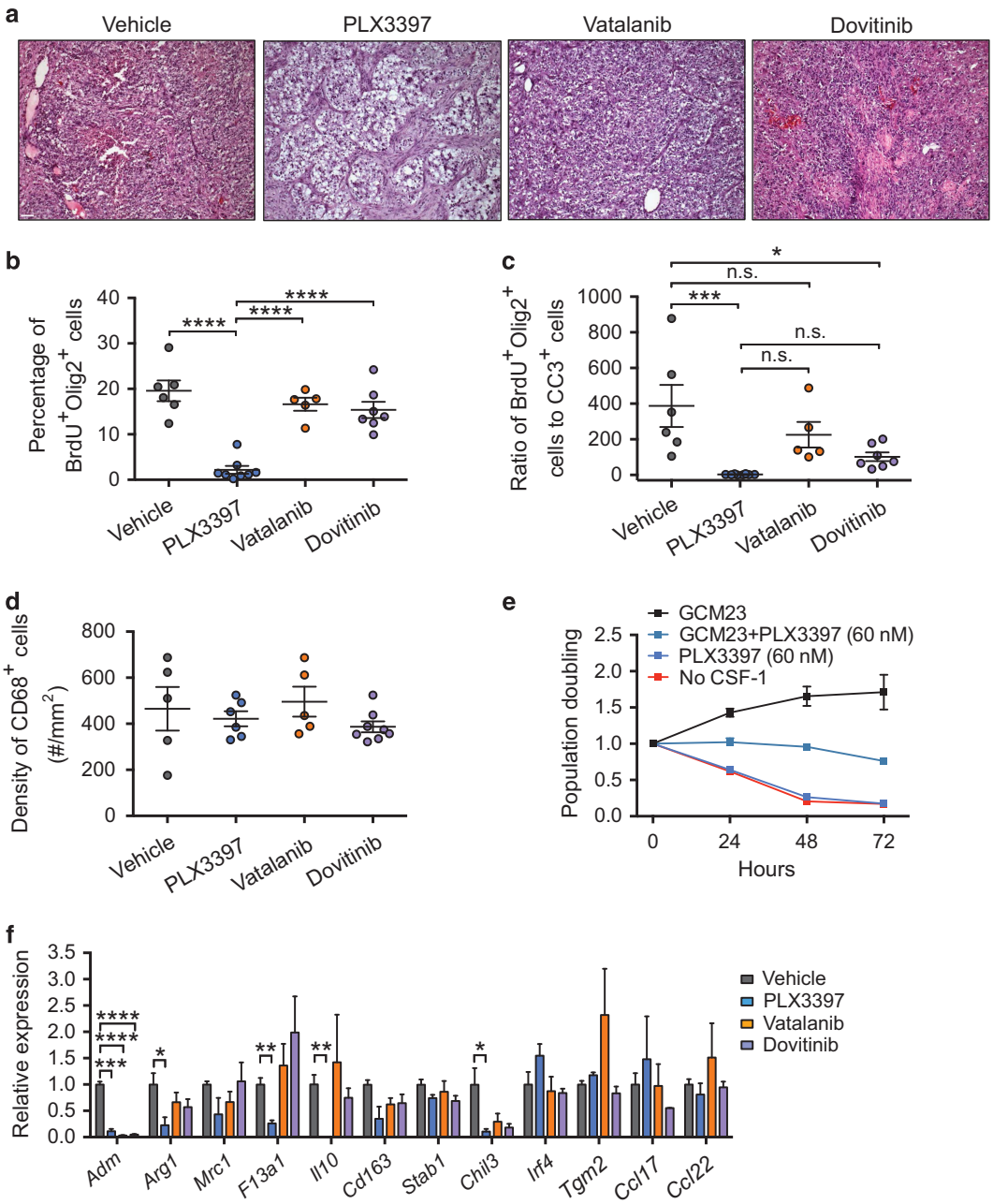

Figure 2. Alterations of malignant features and TAM gene expression in treated gliomas. (**a**) Representative hematoxylin and eosin images of treated tumors from the treatment groups shown in Figures 1c and d. Scale bar, 50 μm. (**b**) Quantification of proliferating tumor cells ($Olig2^+$ $BrdU^+$) in all treatment arms. (**c**) Quantification of the ratio of proliferating tumor cells to apoptotic cells within treated gliomas. (**d**) Quantification of $CD68^+$ TAM density in all treatment arms. (**e**) MTT assay showing cell viability of BMDMs treated with GCM, PLX3397 (60 nM, based on estimated IC_{50} from dose–response studies in Supplementary Figure 2C), or a combination of both. Population doubling was calculated using absorbance values (A_{595}-A_{750}) and time 0 values as normalization factors, $n = 3$ independent experiments. (**f**) Quantification of mRNA expression of M2-like genes, including *Adm*, *Arg1*, *Mrc1*, *F13a1*, *Il10*, *Cd163*, *Stab1*, *Chil3*, *Irf4* and *Ccl22*, in treated gliomas, $n = 3$ tumors. One-way analysis of variance with Sidak's multiple comparisons test was used to calculate statistical significance. $^*P < 0.05$; $^{**}P < 0.01$; $^{***}P < 0.001$; $^{****}P < 0.0001$; n.s. not significant. For **b**, **c**, and **d**, each point represents a different tumor.

PLX3397 alters malignant features of gliomas

To investigate how the RTK inhibitors differentially altered glioma progression *in vivo*, we analyzed tumors after the 7-day trial. Histological analysis revealed that PLX3397 elicited substantial tumor debulking, as indicated by a decrease in intratumoral nuclear density, whereas vatalanib and dovitinib largely failed to do so (Figure 2a). Histological blinded grading based on the 2007 WHO classification system showed that PLX3397 treatment resulted mostly in lesions with grade II morphology (90%), with grade III morphology in the remaining 10%. Grade IV histopathological features were not apparent in this group, in contrast to the vehicle-treated animals in which all lesions scored as grade IV glioblastoma (Supplementary Figure S5A; $P < 0.0001$). By comparison, vatalanib had no effect on glioma grade relative to the vehicle group, and dovitinib treatment resulted in an equivalent distribution of grade IV and grade III gliomas (Supplementary Figure S5A).

We next assessed additional tumorigenic processes including glioma cell proliferation, apoptosis, and the intratumoral

microvasculature. In accordance with the histological changes, PLX3397 dramatically decreased the proportion of Olig2$^+$ glioma cells to 20% of total cells, as compared to 80% in vehicle-treated gliomas (Supplementary Figure S5; $P < 0.0001$). We also pulse-labeled proliferating glioma cells with BrdU *in vivo*, and observed that the percentage of proliferating Olig2$^+$ cells was markedly reduced by 88.9% following PLX3397 treatment compared to the vehicle group (Figure 2b and Supplementary Figure S5B; $P < 0.0001$). By contrast, neither vatalanib nor dovitinib changed the percentage of total Olig2$^+$ cells or actively proliferating glioma cells *in vivo* (Figure 2b and Supplementary Figure S5). Quantification of apoptotic cells using cleaved caspase 3 (CC3) staining showed a significant increase in PLX3397-treated gliomas (Supplementary Figure S5D; $P < 0.0001$). As a result, PLX3397 significantly decreased the tumor cell proliferation-to-apoptosis ratio (Figure 2c; $P < 0.001$). We also observed a modest decrease in the proliferation-to-apoptosis ratio in dovitinib-treated gliomas, which was mainly driven by a slight increase in apoptosis (Figure 2c and Supplementary Figure S5D). To quantify potential changes in the microvasculature, blood vessels were stained using an anti-CD31 antibody. We did not observe significant differences in microvascular density across the treatment groups (Supplementary Figure S5), but there was a significant reduction in vessel length in the dovitinib-treated group compared with the vehicle group (Supplementary Figure S5G; $P < 0.05$). Dovitinib can bind to VEGFR, FGFR and PDGFR, all of which are associated with angiogenesis and vessel maintenance, and thus the decreased vessel length could be attributed to blockade of one or more of these pathways. Together, these findings indicate the enhanced biological efficacy of a CSF-1R inhibition strategy compared to other RTK targets *in vivo*.

PLX3397 induces gene expression changes in TAMs

In the context of CSF-1R blockade using a chemically distinct small molecule inhibitor, BLZ945,[22] we previously reported that TAMs survive (due to the presence of survival factors including GM-CSF and IFNγ in the proneural glioma microenvironment) but are 're-educated', concomitant with reduced expression of M2-like macrophage genes. Similarly, we find here that PLX3397-mediated CSF-1R inactivation did not lead to a decrease in TAM density compared to vehicle-treated gliomas (Figure 2d and Supplementary Figure S6A, top row). Microglia in the adjacent normal brain, however, were almost fully depleted following PLX3397 treatment as expected (Supplementary Figure S6A, bottom row), indicating that the glioma microenvironment specifically promotes TAM survival in the context of CSF-1R blockade, as we have also demonstrated with an independent small molecule inhibitor.[22] Interestingly, TAM density was similarly unchanged in vatalanib-treated and dovitinib-treated gliomas compared to vehicle, while microglia depletion was observed in the adjacent normal brain of these treatment groups (Figure 2d and Supplementary Figure S6A).

To investigate whether the secretion of soluble factors within the glioma microenvironment has a role in macrophage protection from RTK inhibitor-induced killing, we performed BMDM viability assays in culture using glioma-conditioned media (GCM) generated from the PDGC23 cell lines. Without GCM, BMDMs were sensitive to all three RTK inhibitors and were efficiently killed (Figure 2e and Supplementary Figure S6). Incubation with GCM, however, enabled BMDMs to survive in the presence of the individual inhibitors (Figure 2e and Supplementary Figure S6), suggesting that protective factors secreted by glioma cells can render TAMs resistant to RTK inhibitor-mediated cytocidal effects. Indeed, we previously identified GM-CSF, IFN-γ and CXCL10 as glioma cell-secreted factors that keep TAMs alive in the context of BLZ945 treatment.[22] It is possible that these same factors also protect macrophages from killing induced by the different RTK inhibitors assessed here, which will be an interesting point to investigate in future studies.

The viable TAMs remaining after PLX3397 treatment may nonetheless assume a different phenotype, even if these cells are not depleted within the TME. To test this possibility, we analyzed the expression of a gene panel associated with M2-like gene polarization in macrophages/ microglia, using RNA extracted from treated whole gliomas. Specifically, we quantified *Adm*, *Arg1*, *Mrc1*, *F13a1*, *Il10*, *Cd163*, *Stab1* and *Chil3*, several of which had been successfully used to capture TAM-related expression changes in whole gliomas previously.[22] Indeed, PLX3397 led to depolarization of TAMs from their original M2-like state, as indicated by significant downregulation of *Adm* ($P < 0.001$), *Arg1* ($P < 0.05$), *F13a1* ($P < 0.01$), *Il10* ($P < 0.01$) and *Chil3* ($P < 0.05$), compared with the vehicle group (Figure 2f). We did not observe concurrent upregulation of M1-like associated genes in PLX3397-treated gliomas (Supplementary Figure S6D). By contrast, vatalanib and dovitinib only downregulated *Adm* ($P < 0.0001$) (Figure 2f), indicating that TAMs in these treated tumors were largely maintained in an M2-like state.

TAM depolarization can be accompanied by important changes in cellular functions.[22] To determine whether PLX3397 alters the pro-proliferative function of educated macrophages, we performed conditioned media culture experiments that mimic the heterotypic interactions between tumor cells and macrophages. BMDMs were stimulated with GCM in the presence or absence of PLX3397 for 48 h without media change to generate 'processed' GCM (stimulated MΦ CM), which was then applied back on PDGC23 cells in culture (Supplementary Figure S6E). Cell cycle analysis showed that, in response to the factors secreted by glioma cells, CM collected from these stimulated BMDMs subsequently upregulated tumor cell proliferation in a paracrine manner, compared to CM generated by naïve BMDMs (Supplementary Figure S6F, $P < 0.0001$). This positive feedback loop, however, was nearly abolished when macrophage function was altered by the addition of PLX3397 during the BMDM stimulation phase (Supplementary Figure S6F, $P < 0.0001$). Taken together, our data indicate that PLX3397 efficiently impairs the pro-tumorigenic functions of TAMs, which likely contributes to the reduced tumor growth or regression observed *in vivo*.

Combination therapy with PLX3397 and dovitinib or vatalanib enhances therapeutic efficacy

Considering that PLX3397 depolarized TAMs in gliomas, we hypothesized that such phenotypically altered TAMs may render glioma cells more sensitive to vatalanib or dovitinib *in vivo*. Therefore, we treated a cohort of mice (including gliomas $\leqslant 40\ mm^3$ and $> 40\ mm^3$) with a combination of PLX3397 and either vatalanib or dovitinib using the same preclinical trial design as in the single-agent trials (Figure 1a). Analysis of individual tumor volumes by waterfall plots showed that the combination therapy regressed the majority of gliomas to a greater extent than PLX3397 alone. By applying the RECIST criteria of 30% tumor volume reduction, 58.8% of the PLX3397 and vatalanib group, and 76.5% of PLX3397 and dovitinib group surpassed this reduction, compared to 3.7% of tumors in the PLX3397 alone group and none of the tumors in the vatalanib or dovitinib monotherapy groups (Figures 1c and 3a). Statistical analysis revealed that the combination therapies significantly reduced overall tumor volume, and performed better than PLX3397 alone (Figure 3b).

The combination therapies elicited robust and consistent debulking in all gliomas (Figure 4a), which was supported by immunohistochemical analyses (Supplementary Figure S7A; $P < 0.0001$). Furthermore, combined treatments abolished tumor cell proliferation while inducing apoptosis, resulting in generally lower proliferation-to-apoptosis ratios compared with PLX3397 alone, though the difference was not statistically significant

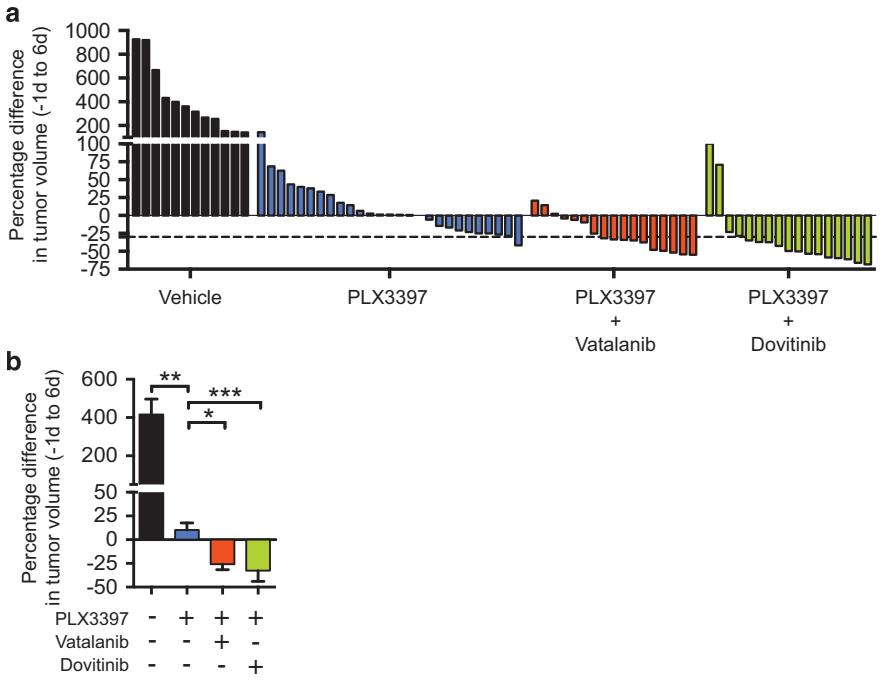

Figure 3. Combination therapy enhances anti-glioma efficacy in the PDG model. (**a**) Waterfall plot showing tumor volume changes in the combination therapy arms: PLX3397+vatalanib ($n = 17$) and PLX3397+dovitinib ($n = 17$), compared with vehicle-treated ($n = 12$) and PLX3397-treated ($n = 27$) gliomas (shown in Figures 1c and d), with RECIST cutoff of 30% regression indicated by the dashed line. (**b**) Tumor volume changes in gliomas receiving combination therapies. Kruskal–Wallis test with Dunn's multiple comparisons test was used to calculate statistical significance. $^{*}P < 0.05$; $^{**}P < 0.01$; $^{***}P < 0.001$.

(Figures 4b and c and Supplementary Figure S7B and C). However, we observed some sporadic high-grade features, such as pseudopalisading necrosis (data not shown), and a higher microvascular density and vessel length in the PLX3397 plus vatalanib group, though not the PLX3397 plus dovitinib group (Supplementary Figure S7D–F). These data suggest that in the PDG model of proneural glioblastoma, destruction of the intratumoral vascular network is not required for achieving glioma regression. In the single-agent setting, microvascular density and vessel length were unchanged after 7 days of PLX3397 treatment. By contrast, dovitinib alone significantly decreased vessel length without a pronounced anti-glioma activity. In the combination therapy setting, PLX3397 plus vatalanib resulted in a significant increase in microvascular density and vessel length, despite a potent anti-glioma effect. Collectively, these findings indicate an apparent disconnect between tumor regression and vascular alterations, at least as assessed in end-stage lesions. Nonetheless, agents that are capable of inducing more extensive vascular damage within gliomas may still add benefit to a CSF-1R inhibitor combination therapy.

TAM density modestly increased compared with vehicle-treated gliomas (Figure 4d and Supplementary Figure S8A; $P < 0.05$), indicating that the therapeutic efficacy was not achieved via TAM depletion. Indeed, compared with PLX3397 monotherapy, we found that combination therapies further downregulated M2-like gene expression of *Stab1, Irf4* and *Ccl22* (Figure 4e), though without inducing M1-like genes (Supplementary Figure S8B). Taken together, our findings demonstrate that concurrent targeting of glioma cells and TAMs in their local microenvironment significantly improves therapeutic efficacy.

DISCUSSION

In this preclinical study, we demonstrate that treatment with the CSF-1R inhibitor PLX3397 is sufficient to block glioma progression in a single-agent setting. Specifically, we observed that PLX3397 induces TAM depolarization from an M2-like state, which is similar to our previous finding using the chemically distinct CSF-1R inhibitor, BLZ945.[22] Furthermore, we found that PLX3397 effectively improves the efficacy of the multi-targeted kinase inhibitors vatalanib and dovitinib *in vivo*, resulting in pronounced glioma regression following combination treatments.

Our findings underscore the utility of TAM plasticity as a therapeutic target in the glioma microenvironment. As evidenced by our results herein from single-agent preclinical trials, appropriately reprogrammed TAMs not only lose their pro-tumorigenic functions but also actively exert anti-tumoral effects. Underlying this phenotypic switch is the downregulation of a subset of genes that are associated with the M2-like state of TAMs. Genes such as *Arg1*, *Il10* and *Chil3* have been implicated in TAM M2 polarization across multiple cancers.[31] The phenotypic alteration of TAMs consequently renders glioma cells more susceptible to pharmacological inhibition of mitogenic RTKs, which provides an opportunity to maximize therapeutic outcomes via combination therapies. Interestingly, we found that combination therapies further downregulated M2-associated genes such as *Mrc1*, *Stab1* and *Ccl22*. Thus, TAM reprogramming potentially represents a more effective strategy than TAM depletion for treating proneural glioblastomas.

The differences between the efficacy of multi-targeted RTK inhibitors *in vitro* versus treatment *in vivo* suggests that pro-tumorigenic TAMs may blunt the effectiveness of these therapies in glioblastoma. Our data show that both vatalanib and dovitinib are capable of efficiently arresting glioma cell proliferation and inducing cell death in a monoculture setting, thus indicating the presence of a cell-extrinsic resistance mechanism *in vivo*. Because TAMs have been shown to interfere with the efficacy of chemotherapy and radiotherapy (reviewed in De Palma *et al.*,[32] Ruffell *et al.*,[33]), it would be of interest to determine whether TAMs also exert such an effect against RTK inhibitors in other tumor types. The demonstrated efficacy of combination therapies herein suggests that TAM reprogramming by CSF-1R inhibition can

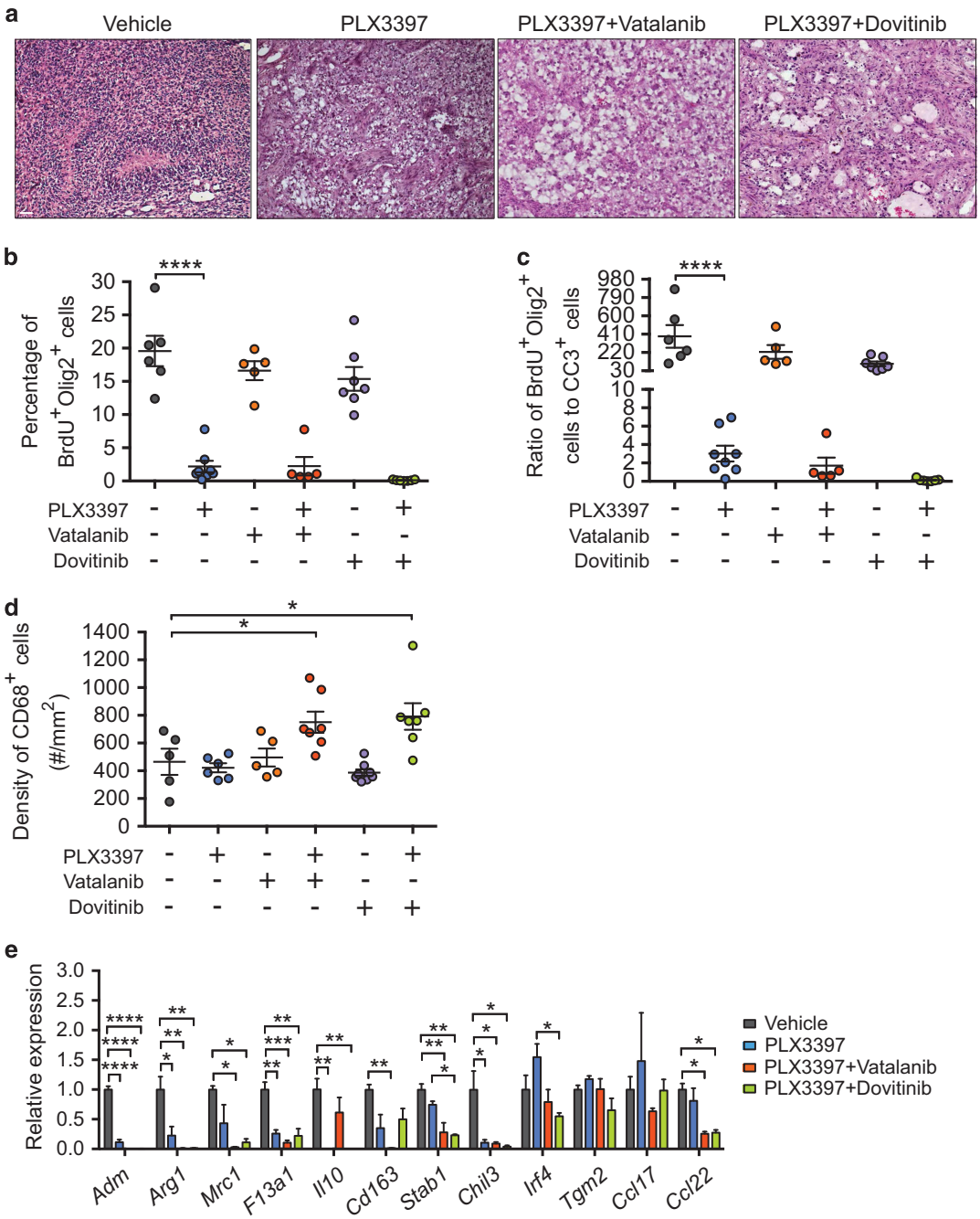

Figure 4. Alterations of malignant features and TAM gene expression in gliomas treated with combination therapy. (**a**) Representative hematoxylin and eosin images of gliomas in the vehicle, PLX3397, PLX3397+vatalanib, and PLX3397+dovitinib arms. Scale bar, 50 μm. (**b**) Quantification of tumor cell proliferation ($Olig2^+$ $BrdU^+$). (**c**) Quantification of the ratio of proliferating tumor cells to apoptotic cells within gliomas. (**d**) Quantification of $CD68^+$ TAM density. Values in the single-agent groups are from Figures 2b-d for comparison purposes. (**e**) Quantification of mRNA expression of M2-like genes, including *Adm*, *Arg1*, *Mrc1*, *F13a1*, *Il10*, *Cd163*, *Stab1*, *Chil3*, *Irf4* and *Ccl22*, in treated gliomas, $n = 3$ tumors. One-way analysis of variance with Sidak's multiple comparisons test was used to calculate statistical significance. $^*P < 0.05$; $^{**}P < 0.01$; $^{***}P < 0.001$; $^{****}P < 0.0001$; n.s. not significant. For **b**, **c** and **d** each point represents a different tumor.

overcome primary or intrinsic resistance to multi-targeted RTK inhibitors in glioblastomas, and thus warrants reconsideration of these inhibitors in glioblastoma treatment in a combinatorial setting. Because PLX3397 and some multi-targeted inhibitors, such as dovitinib, have advanced through phase I clinical trials in recurrent glioblastoma patients,[34,35] it would be timely to explore whether such combination therapies can improve clinical outcomes in patients with newly diagnosed or recurrent glioblastoma. In parallel, it will be important to determine whether PLX3397 also provides therapeutic benefits in non-proneural glioblastoma, where multiple RTK inhibitors can potentially be utilized to perturb oncogenic pathways.

MATERIALS AND METHODS

Generation of PDGF-B-driven murine gliomas

The Nestin-Tv-a *Ink4a/Arf*$^{-/-}$ mouse line has been described previously[27] and was generously provided by Dr Eric Holland. Briefly, to initiate gliomas, mice at

5-6 weeks of age (males and females) were intracranially injected with DF1 cells harboring the replication-competent avian retrovirus-hPDGF-B-HA virus, using a fixed stereotactic apparatus (Stoelting, Wood Dale, IL, USA) under full anesthesia with ketamine and xylazine. The injection was performed at a depth of 2 mm into the right front cortex, using a coordinate that was 1.5 mm lateral and 1 mm caudal from bregma, as previously described.[22,36]

Glioma regression trial

The size of cohorts was estimated based on our previous experience with the genetically engineered PDG mouse model.[22,36] All the experimental animals enrolled were included in the tumor burden analyses, which were conducted in a non-blinded manner. One day before treatment started (4.5–5.5 weeks post-tumor initiation), PDG mice were scanned by magnetic resonance imaging to measure tumor volume. Tumor-bearing mice with gliomas $\leqslant 40\ mm^3$ were then randomized into different groups to receive either vehicle or tyrosine kinase inhibitors. Mice with gliomas $>40\ mm^3$ were treated with PLX3397 or combination therapy, except for two mice treated with vehicle. The vehicle for PLX3397 consists of 0.5% HPMC, 1% PS80 and 5% DMSO. The vehicle for vatalanib and dovitinib is sterile water. Mice were orally dosed by gavage once daily, and received PLX3397 (100 mg/kg), vatalanib (100 mg/kg) or dovitinib (120 mg/kg). For the combination trials, mice were administered PLX3397 (100 mg/kg) and either vatalanib (100 mg/kg) or dovitinib (120 mg/kg), 40 min apart. All enrolled animals were scanned by magnetic resonance imaging on day 6, and relative tumor volume changes were calculated compared to day − 1. Unless otherwise indicated, mice were given the last dose of inhibitors 4 h before sacrifice at the end of day 7. For each mouse whose tissue was collected for immunohistochemical analyses, a dose of BrdU (100 mg/kg) was injected intraperitoneally 2 h before sacrifice. All animal studies were approved by the Institutional Animal Care and Use Committee of MSKCC.

Harvesting of mouse tissues

PDG mice were euthanized 7 days after treatment was initiated. Before tissue harvest, each mouse was administered a lethal dose of avertin (2,2,2-tribromoethanol, Sigma, St Louis, MO, USA), followed by transcardiac perfusion with phosphate-buffered saline (PBS). To harvest tissues for immunohistochemical analyses, each mouse was subsequently perfused with 4% paraformaldehyde in PBS. Brains were fixed in 4% paraformaldehyde overnight at 4 °C and transferred to 30% sucrose at 4 °C the next day. All the other tissues were placed in 30% sucrose at 4 °C directly following paraformaldehyde perfusion. After reaching equilibrium in sucrose, all tissues were embedded in OCT compound (Tissue-Tek, Torrance, CA, USA). To collect tissues for RNA and protein extraction, gliomas were carefully dissected and snap frozen immediately following transcardial PBS perfusion.

Pharmacokinetic analysis

Non-tumor-bearing Nestin-Tv-a *Ink4a/Arf*$^{-/-}$ mice at 5 weeks of age were orally administered a single dose of PLX3397 (100 mg/kg), vatalanib (100 mg/kg) or dovitinib (120 mg/kg). After 2 h, mice were euthanized for plasma and cerebellum collection. Samples were stored at − 80 °C and sent to Integrated Analytical Solutions (Berkeley, CA, USA) for quantitative analysis.

Histology and immunofluorescence analyses

10 μm frozen sections were used for all analyses. For histological assessment, hematoxylin and eosin staining was performed, and histopathology was blindly scored by a neuropathologist (Dr Jason Huse) based on the 2007 WHO criteria.[37] For immunofluorescence analyses, dried frozen sections were rehydrated in PBS, permeabilized in 0.2% Triton X-100, and blocked in 0.5% PNB (PerkinElmer, Waltham, MA, USA) for 1 h at room temperature. Sections were then incubated with primary antibody (for antibody information, see Supplementary Table 1) in 0.25% PNB at 4 °C overnight, followed by PBS washes and incubation with fluorophore-conjugated secondary antibody (Life Technologies, Carlsbad, CA, USA) in 0.25% PNB for 1 h at room temperature. After repeated washes and counterstaining with DAPI, sections were mounted with ProLong Gold Antifade mounting media (Life Technologies). Stained tissue sections were visualized under a Carl Zeiss (Thornwood, NY, USA) Axioimager Z1 microscope equipped with a TissueGnostics (Tarzana, CA; USA) scanning stage or a Carl Zeiss Axioscan Z1 microscope equipped with Zen 2.3 software (Thornwood, NY, USA). Quantification of intratumoral changes was performed using TissueQuest and StrataQuest software (TissueGnostics), as previously described.[22]

Generation of primary mouse bone marrow-derived macrophages (BMDMs)

Wild-type C57BL/6 mice (6–8 weeks old) were euthanized by CO_2. Hind limbs were dissected, and bone marrow was flushed out of the femur and tibia using serum-free DMEM. Bone marrow-derived cells were allowed to differentiate in DMEM with 10% fetal bovine serum and CSF-1 (10 ng/ml) for 7 days, with media change and CSF-1 supplementation every other day. BMDMs were then used in subsequent *in vitro* experiments.

Generation of primary human monocyte-derived macrophages (MDMs)

Peripheral blood mononuclear cells were isolated by density gradient isolation using Ficoll (GE Healthcare, Aurora, OH, USA) from fresh buffy coats donated by consented healthy donors to the Swiss blood transfusion service. Experiments were conducted in accordance to the guidelines of the Ethics Commission of the University of Lausanne, Switzerland. Monocytes were isolated by positive selection using magnetic beads targeting human CD14 (Miltenyi, Auburn, CA, USA). Cells were allowed to differentiate in DMEM supplemented with 10% fetal bovine serum and 10 ng/ml CSF-1 (R&D Systems) for 6 days, with media change and CSF-1 supplementation every other day. MDMs were then used in subsequent *in vitro* experiments.

Cell culture

The generation and characterization of the PDGC23 glioma cell line has been previously described.[22] The U-87MG cell line was provided by Prof. Monika Hegi's lab (University of Lausanne, Switzerland). The cell lines were grown in DMEM supplemented with 10 and 5% fetal bovine serum, respectively. Both cell lines were routinely screened for mycoplasma.

Conditioned media experiments

To generate glioma-conditioned media (GCM), 5×10^6 PDGC23 cells were incubated in 12 ml serum-free DMEM for 24 h. Harvested GCM was passed through 0.22 μm filters to remove debris, and used to perform BMDM protection assays in the presence of inhibitors. GCM was also used to stimulate BMDMs (in the absence of CSF-1) for 48 h to produce 'stimulated' MΦ CM. Vehicle (DMSO) or PLX3397 (60 nM) was added during BMDM stimulation to assess the effect of PLX3397.

Protein extraction and western blotting

To isolate protein from primary BMDMs and PDGC23 cells, lysis was performed in NP-40 buffer containing protease and phosphatase inhibitors (Thermo Scientific, Waltham, MA, USA). Protein extraction from MDMs and U-87MG cells was performed with RIPA buffer (Sigma) containing protease and phosphatase inhibitors (Thermo Scientific). To extract protein from dissected gliomas, a pre-established biochemical fractionation protocol was used.[22,38] The resultant synaptosomal membrane fraction was lysed in NP-40 buffer as described above. Extracted protein was resolved in 4-12% Bis-Tris SDS-PAGE gels (Life Technologies), transferred to PVDF membrane (Millipore, Billerica, MA, USA), and blocked with 5% non-fat milk. Membranes were incubated overnight at 4 °C with primary antibodies (Cell Signaling Technology, Danvers, MA, USA) against phosphorylated-PDGFRα (Y762), phosphorylated-CSF-1R (Y723), total PDGFRα or total CSF-1R (for antibody information, see Supplementary Table 1). Following incubation with horseradish peroxidase-conjugated secondary antibody (dilution 1:5000) for 1 h at room temperature, target protein was detected using a chemiluminescence system (Thermo Scientific).

Cell cycle and cell death analysis

To determine the effect of tyrosine kinase inhibitors on glioma cells, PDGC23 cells were treated with vatalanib (1, 5, 20 μM) or dovitinib (0.5, 1, 5 μM) for up to 48 h in serum-free DMEM. U-87MG cells were treated with vatalanib (1, 10, 50 μM) or dovitinib (0.5, 1, 5 μM) in serum-free DMEM for 48 h. For conditioned media experiments (CM), PDGC23 cells were incubated with stimulated MΦ CM for 48 h. Then cells were dissociated by trypsinization, washed, and stained with LIVE/DEAD fixable dye (near-IR, Life Technologies) or Zombie NIR Viability kit (Biolegend, San Diego, CA, USA). Cells were then permeabilized and stained with DAPI to allow for simultaneous cell cycle analysis. After acquisition on a LSR II flow cytometer (BD, Franklin Lakes, NJ, USA), cell cycle stage and cell death were analyzed using Flow Jo software (Ashland, OR, USA). Cell cycle was analyzed using the Dean Jett Fox model.

Cell viability assay

MTT assays were performed using the Cell Proliferation Kit I (Roche) according to the manufacturer's instructions. BMDMs and MDMs were seeded at 7×10^3 cells/well and 20×10^3 cells/well respectively, incubated in DMEM with 10% fetal bovine serum and CSF-1 (10 ng/ml) throughout the experiments. PDGC23 and U-87MG cells were seeded at 4×10^3 cells/well and 10×10^3 cells/well respectively, incubated in serum-free DMEM until the end point. All experimental assays were performed at the 48-h time point. For U-87MG and MDM assays, values correspond to the difference between absorbance at 560 and 690 nm, while for BMDMs and PDGC23 cell assays absorbance was acquired at 595 and 750 nm.

RNA isolation, cDNA synthesis and qPCR

RNA was extracted using TRIzol (Life Technologies). For cDNA synthesis, the Transcriptor First Strand cDNA Synthesis Kit (Roche) was used with 1 μg of RNA. TaqMan probes (Life Technologies) for *Ubc* (Mm01201237_m1), *Adm* (Mm00437438_g1), *Arg1* (Mm00475988_m1), *Mrc1* (Mm00485148_m1), *F13a1* (Mm00472334_m1), *Il10* (Mm00439614_m1), *Cd163* (Mm00474091_m1), *Stab1* (Mm00460390_m1), *Chil3* (Mm00657889_mH), *Irf4* (Mm00516431_m1), *Ccl22* (Mm00436439_m1), *Nos2* (Mm00440502_m1), *Ptgs2* (Mm00478374_m1), *Il1b* (Mm00434228_m1), *Il12b* (Mm00434174_m1), *Ccl2* (Mm00441242_m1), *Ccl5* (Mm01302427_m1) and *Cxcl10* (Mm00445235_m1) were used for qPCR. Assays were performed in triplicate and relative expression was calculated after normalization to the housekeeping gene *Ubc* for each sample.

Statistical analysis

Data are presented throughout as mean and ± s.e.m, analyzed by the indicated tests and a significance cutoff of $P < 0.05$. All statistical analyses were completed in GraphPad Prism 6.0 or 7.0 (La Jolla, CA, USA).

CONFLICT OF INTEREST

BLW is an employee of Plexxikon Inc, which provided the PLX3397 compound. The remaining authors declare no conflict of interest.

ACKNOWLEDGEMENTS

We thank Dr Florian Klemm and all members of the Joyce laboratory for insightful comments and experimental advice. We are grateful to Kenishana Simpson, Xiaoping Chen and Nisarg Shah for excellent technical support. We thank Dr Eric Holland for scientific discussion, and for generously providing the Nestin-Tv-a *Ink4a/Arf*$^{-/-}$ mouse line. This research was supported by the US National Cancer Institute (NCI) (R01CA181355, JAJ), the Swiss Cancer League (KFS 3990-08-2016, JAJ), the Ludwig Institute for Cancer Research (JAJ), NCI Support Grant for the MSKCC core facilities used (P30 CA008748), and the American Brain Tumor Association (LA).

AUTHOR CONTRIBUTIONS

DY and JAJ conceived of the study, designed experiments and analyzed the data. DY, JK, LA and AJS performed and analyzed experiments. JTH performed histopathological analyses. BLW provided PLX3397. DY, JK and JAJ wrote the manuscript. All authors commented on the manuscript, and JAJ supervised the study.

REFERENCES

1 Stupp R, Mason WP, van den Bent MJ, Weller M, Fisher B, Taphoorn MJ *et al.* Radiotherapy plus concomitant and adjuvant temozolomide for glioblastoma. *N Engl J Med* 2005; **352**: 987–996.
2 Verhaak RG, Hoadley KA, Purdom E, Wang V, Qi Y, Wilkerson MD *et al.* Integrated genomic analysis identifies clinically relevant subtypes of glioblastoma characterized by abnormalities in PDGFRA, IDH1, EGFR, and NF1. *Cancer Cell* 2010; **17**: 98–110.
3 Dunn GP, Rinne ML, Wykosky J, Genovese G, Quayle SN, Dunn IF *et al.* Emerging insights into the molecular and cellular basis of glioblastoma. *Genes Dev* 2012; **26**: 756–784.
4 Quail DF, Joyce JA. The microenvironmental landscape of brain tumors. *Cancer Cell* 2017; **31**: 326–341.
5 Brennan C, Momota H, Hambardzumyan D, Ozawa T, Tandon A, Pedraza A *et al.* Glioblastoma subclasses can be defined by activity among signal transduction pathways and associated genomic alterations. *PLoS One* 2009; **4**: e7752.
6 Mellinghoff IK, Schultz N, Mischel PS, Cloughesy TF. Will kinase inhibitors make it as glioblastoma drugs? *Curr Top Microbiol Immunol* 2012; **355**: 135–169.
7 Geng L, Shinohara ET, Kim D, Tan J, Osusky K, Shyr Y *et al.* STI571 (Gleevec) improves tumor growth delay and survival in irradiated mouse models of glioblastoma. *Int J Radiat Oncol Biol Phys* 2006; **64**: 263–271.
8 Wen PY, Yung WK, Lamborn KR, Dahia PL, Wang Y, Peng B *et al.* Phase I/II study of imatinib mesylate for recurrent malignant gliomas: North American Brain Tumor Consortium Study 99-08. *Clin Cancer Res* 2006; **12**: 4899–4907.
9 Ziegler DS, Wright RD, Kesari S, Lemieux ME, Tran MA, Jain M *et al.* Resistance of human glioblastoma multiforme cells to growth factor inhibitors is overcome by blockade of inhibitor of apoptosis proteins. *J Clin Invest* 2008; **118**: 3109–3122.
10 Paul I, Bhattacharya S, Chatterjee A, Ghosh MK. Current understanding on EGFR and Wnt/beta-Catenin signaling in glioma and their possible crosstalk. *Genes Cancer* 2013; **4**: 427–446.
11 Beier D, Schulz JB, Beier CP. Chemoresistance of glioblastoma cancer stem cells--much more complex than expected. *Mol Cancer* 2011; **10**: 128.
12 Chen J, Li Y, Yu TS, McKay RM, Burns DK, Kernie SG *et al.* A restricted cell population propagates glioblastoma growth after chemotherapy. *Nature* 2012; **488**: 522–526.
13 Agarwal S, Mittapalli RK, Zellmer DM, Gallardo JL, Donelson R, Seiler C *et al.* Active efflux of Dasatinib from the brain limits efficacy against murine glioblastoma: broad implications for the clinical use of molecularly targeted agents. *Mol Cancer Ther* 2012; **11**: 2183–2192.
14 Shi H, Hugo W, Kong X, Hong A, Koya RC, Moriceau G *et al.* Acquired resistance and clonal evolution in melanoma during BRAF inhibitor therapy. *Cancer Discov* 2014; **4**: 80–93.
15 Bowman RL, Klemm F, Akkari L, Pyonteck SM, Sevenich L, Quail DF *et al.* Macrophage ontogeny underlies differences in tumor-specific education in brain malignancies. *Cell Rep* 2016; **17**: 2445–2459.
16 Charles NA, Holland EC, Gilbertson R, Glass R, Kettenmann H. The brain tumor microenvironment. *Glia* 2012; **60**: 502–514.
17 Reardon DA, Freeman G, Wu C, Chiocca EA, Wucherpfennig KW, Wen PY *et al.* Immunotherapy advances for glioblastoma. *Neuro Oncol* 2014; **16**: 1441–1458.
18 Kennedy BC, Showers CR, Anderson DE, Anderson L, Canoll P, Bruce JN *et al.* Tumor-associated macrophages in glioma: friend or foe? *J Oncol* 2013; **2013**: 486912.
19 Komohara Y, Ohnishi K, Kuratsu J, Takeya M. Possible involvement of the M2 anti-inflammatory macrophage phenotype in growth of human gliomas. *J Pathol* 2008; **216**: 15–24.
20 Hussain SF, Yang D, Suki D, Aldape K, Grimm E, Heimberger AB. The role of human glioma-infiltrating microglia/macrophages in mediating antitumor immune responses. *Neuro Oncol* 2006; **8**: 261–279.
21 Engler JR, Robinson AE, Smirnov I, Hodgson JG, Berger MS, Gupta N *et al.* Increased microglia/macrophage gene expression in a subset of adult and pediatric astrocytomas. *PLoS One* 2012; **7**: e43339.
22 Pyonteck SM, Akkari L, Schuhmacher AJ, Bowman RL, Sevenich L, Quail DF *et al.* CSF-1R inhibition alters macrophage polarization and blocks glioma progression. *Nat Med* 2013; **19**: 1264–1272.
23 DeNardo DG, Brennan DJ, Rexhepaj E, Ruffell B, Shiao SL, Madden SF *et al.* Leukocyte complexity predicts breast cancer survival and functionally regulates response to chemotherapy. *Cancer Discov* 2011; **1**: 54–67.
24 Tap WD, Wainberg ZA, Anthony SP, Ibrahim PN, Zhang C, Healey JH *et al.* Structure-guided blockade of CSF1R kinase in tenosynovial giant-cell tumor. *N Engl J Med* 2015; **373**: 428–437.
25 Wood JM, Bold G, Buchdunger E, Cozens R, Ferrari S, Frei J *et al.* PTK787/ZK 222584, a novel and potent inhibitor of vascular endothelial growth factor receptor tyrosine kinases, impairs vascular endothelial growth factor-induced responses and tumor growth after oral administration. *Cancer Res* 2000; **60**: 2178–2189.
26 Trudel S, Li ZH, Wei E, Wiesmann M, Chang H, Chen C *et al.* CHIR-258, a novel, multitargeted tyrosine kinase inhibitor for the potential treatment of t(4;14) multiple myeloma. *Blood* 2005; **105**: 2941–2948.
27 Dai C, Celestino JC, Okada Y, Louis DN, Fuller GN, Holland EC. PDGF autocrine stimulation dedifferentiates cultured astrocytes and induces oligodendrogliomas and oligoastrocytomas from neural progenitors and astrocytes *in vivo*. *Genes Dev* 2001; **15**: 1913–1925.
28 Shih AH, Dai C, Hu X, Rosenblum MK, Koutcher JA, Holland EC. Dose-dependent effects of platelet-derived growth factor-B on glial tumorigenesis. *Cancer Res* 2004; **64**: 4783–4789.

29 Uhrbom L, Nerio E, Holland EC. Dissecting tumor maintenance requirements using bioluminescence imaging of cell proliferation in a mouse glioma model. *Nat Med* 2004; **10**: 1257–1260.
30 Lee SH, Lopes de Menezes D, Vora J, Harris A, Ye H, Nordahl L *et al*. *In vivo* target modulation and biological activity of CHIR-258, a multitargeted growth factor receptor kinase inhibitor, in colon cancer models. *Clin Cancer Res* 2005; **11**: 3633–3641.
31 Biswas SK, Mantovani A. Macrophage plasticity and interaction with lymphocyte subsets: cancer as a paradigm. *Nat Immunol* 2010; **11**: 889–896.
32 De Palma M, Lewis CE. Macrophage regulation of tumor responses to anticancer therapies. *Cancer Cell* 2013; **23**: 277–286.
33 Ruffell B, Coussens LM. Macrophages and therapeutic resistance in cancer. *Cancer Cell* 2015; **27**: 462–472.
34 Butowski N, Colman H, De Groot JF, Omuro AM, Nayak L, Wen PY *et al*. Orally administered colony stimulating factor 1 receptor inhibitor PLX3397 in recurrent glioblastoma: an Ivy Foundation Early Phase Clinical Trials Consortium phase II study. *Neuro Oncol* 2016; **18**: 557–564.
35 Schafer N, Gielen GH, Kebir S, Wieland A, Till A, Mack F *et al*. Phase I trial of dovitinib (TKI258) in recurrent glioblastoma. *J Cancer Res Clin Oncol* 2016; **142**: 1581–1589.
36 Quail DF, Bowman RL, Akkari L, Quick ML, Schuhmacher AJ, Huse JT *et al*. The tumor microenvironment underlies acquired resistance to CSF-1R inhibition in gliomas. *Science* 2016; **352**: *aad3018*.
37 Louis DN, Ohgaki H, Wiestler OD, Cavenee WK, Burger PC, Jouvet A *et al*. The 2007 WHO classification of tumours of the central nervous system. *Acta Neuropathol* 2007; **114**: 97–109.
38 Hallett PJ, Collins TL, Standaert DG, Dunah AW. Biochemical fractionation of brain tissue for studies of receptor distribution and trafficking. *Curr Protoc Neurosci* 2008; **Chapter 1**: Unit 1,16.

Supplementary Information accompanies this paper on the Oncogene website (http://www.nature.com/onc)